PAPER

Check for updates

Hybrid-functional calculations of electronic structure and phase stability of MO (M = Zn, Cd, Be, Mg, Ca, Sr, Ba) and related ternary alloy $M_xZn_{1-x}O$

Jinying Yu,[a] Mingke Zhang,[a] Zihan Zhang,[bc] Shangwei Wang[a] and Yelong Wu (iD) *[bc]

Using the hybrid exchange–correlation functional within the density-functional theory, we have systematically investigated the structural and electronic properties of MO (M = Be, Mg, Ca, Sr, Ba, Zn, Cd) in binary rock salt (B1), zinc-blende (B3) and wurtzite (B4) phases, including the structural parameters, bulk moduli, band gaps and deformation potentials. Our results agree well with the experimental data and other theoretical results, and give a better understanding of the relationship between the geometric and electronic structure. After calculating the band alignment, we find that in both the B1 and B3 structures, the valence band maximum (VBM) has an obvious decrease from BeO to MgO to CaO, then it goes up from SrO to BaO to ZnO to CdO. Moreover, the properties of the ternary alloys $M_xZn_{1-x}O$ were studied through the application of the special quasi-random structure method. The critical value of the ZnO composition for the transition from the B3 structure to the B1 structure gradually increases from (Ca, Zn)O to (Mg, Zn)O to (Sr, Zn)O to (Ba, Zn)O to (Cd, Zn)O, indicating that (Ca, Zn)O can exist in the B3 structure with the lowest ZnO composition. These results provide a good guideline for the accessible phase space in these alloy systems.

I. Introduction

Low toxicity, stable quality and earth-abundance are the important criteria for choosing materials for practical devices. Oxygen is earth-abundant and it forms stable chemical bonds with almost all elements to give the corresponding oxides, which are generally stable in the ambient atmosphere and water. They are much safer than chalcogens and pnictogens, such as sulfur, selenium, arsenic and antimony. These advantages draw interest to oxides as safe and environmentally conscious materials. Oxide semiconductors, such as ZnO,[1,2] TiO2,[3,4] In2O3 (ref. 5 and 6) and SnO2,[7] have been studied quite extensively by combining experiment and theory in the past decades, and they currently play an important role in inorganic functional materials. Generally, oxide semiconductors have a sufficiently wide band gap to be transparent to visible light. They are widely used in transparent electrodes and transparent film transistors (TFTs), such as In2O3:Sn,[8] SnO2:F,[9] ZnO:Al,[10] and CuGaO2.[11,12] However, most oxide semiconductors have a B1 rock salt structure ($Fm\bar{3}m$), where the cation atom adopt octahedral coordination, see Fig. 1. They do not have a direct

band gap (due to the coupling between the cation d states with O 2p away from Γ in a centrosymmetric O_h environment), *i.e.*, they are not appropriate to be applied in active optoelectronic devices, such light-emitting diodes (LEDs) and photovoltaics.

Compound semiconductors with cubic B3 zinc-blende ($F\bar{4}3m$) and hexagonal B4 wurtzite structure ($P6_3mc$), where each cation atom adopts tetrahedral coordination, see Fig. 1, usually have a direct allowed band gap.[13–15] Among the binary oxide semiconductors, ZnO is the only semiconductor with a hexagonal B4 wurtzite structure that has a direct allowed band gap, except for the carcinogenic BeO.[16,17] Moreover, its cubic B3 zinc-blende polymorph lies slightly higher in energy due to the reduced Madelung constant. The nature of its direct band gap makes ZnO an attractive material for optoelectronic applications.[18] However, the band gap of ZnO is about 3.4 eV, which is in the near ultraviolet (UV) region. Greater flexibility in emission wavelengths for ZnO-based optoelectronic devices is highly
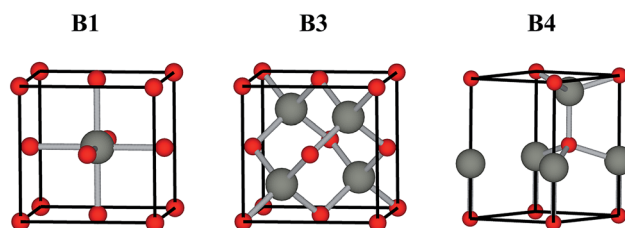
[a]School of Physics, Northwest University, Xi'an, Shaanxi, 710069, China

[b]Key Laboratory of Nonequilibrium Synthesis and Modulation of Condensed Matter (Xi'an Jiaotong University), Ministry of Education, Xi'an, Shaanxi 710049, China. E-mail: yelongwu@xjtu.edu.cn

[c]Shaanxi Key Laboratory of Quantum Information and Quantum Optoelectronic Devices, Xi'an Jiaotong University, Xi'an, Shaanxi 710049, China

Fig. 1 Conventional unit cells of the B1 rock salt, B3 zinc-blende, B4 wurtzite structures.

demanded.[19] The binary oxides MO (M = Cd, Be, Mg, Ca, Sr, Ba) and related ternary alloys $M_xZn_{1-x}O$ are generating considerable interest, because they can provide, in principle, an accessible direct band gap range from visible light to deep UV.[20–23] However, the binary oxide semiconductors that possess the B3 structure are limited to ZnO. Therefore, the band gap engineering of ZnO by alloying with MOs is difficult compared to II–VI chalcogenide and III–V pnictide semiconductors. Many issues remaining currently hinder the widespread application, one of which is the sensitive structure composition dependence, *i.e.*, alloy formation in this system is greatly affected by segregation outside certain stable compositional ranges. At various alloy compositions and experimental conditions, alloys $M_xZn_{1-x}O$ with B1, B3 and B4 structures are observed. Thus, to understand more about the alloy properties, it is essential and important to study the electronic structure and band alignment of the binary oxides in each crystal structure.

In this work, the electronic structure and phase stability of MO (M = Be, Mg, Ca, Sr, Ba, Zn, Cd) and related ternary alloy $M_xZn_{1-x}O$ in the B1, B3 and B4 phases were investigated *via* density-functional theory calculations using hybrid exchange–correlation functional. The calculated lattice constants, relative total energies and band gaps agree well with the experimental data and other theoretical results. By analyzing the band-gap deformation potentials and band-edge alignment, we found that in both the B1 and B3 structures, the valence band maximum (VBM) has an obvious decrease from BeO to MgO to CaO, then it goes up from SrO to BaO to ZnO to CdO. The lattice mismatch, band-gap bowing parameter and formation energy of ternary alloy $M_xZn_{1-x}O$ were also studied through the application of the special quasi-random structure method. The phase transition from the B3 structure to the B1 structure is predicted with decreasing of the ZnO composition. The critical point of the transition gradually increases from (Ca, Zn)O to (Mg, Zn)O to (Sr, Zn)O to (Ba, Zn)O to (Cd, Zn)O, indicating that (Ca, Zn)O can exist in the B3 structure with the lowest ZnO composition.

II. Calculation methods

Our calculations were performed by using density functional theory (DFT) based on the plane-wave pseudopotential method,[25] as implemented in the Vienna *ab initio* simulation package (VASP).[26–29] It is well known that the accuracy of the calculated band gap E_g depends on the functional. In this study, we choose the Heyd–Scuseria–Ernzerhof (HSE06) hybrid functional,[30] which is widely used for semiconductor calculations and considered to be more accurate than standard local density approximation (LDA) or generalized gradient approximation (GGA).[31,32] In this hybrid method, the exchange–correlation energy is calculated from the hybrid functional between the DFT exchange–correlation functional with Perdew–Burke–Ernzerhof (PBE) parametrization and the Hartree–Fock (HF) exchange integral.[33,34] The mixing parameter α, *i.e.*, the portion of the non-local Fock-exchange energy is normally chosen to be 0.25. However, for most oxide semiconductors or transition metal compounds, the calculated E_g is not predicted accurately

enough, *e.g.*, the experimental E_g of ZnO is reproduced more accurately by increasing α from original 0.25 to 0.375.[35] Moreover, with the modified α, the lattice constants a and c of ZnO turn to 3.24 Å and 5.21 Å, which still agree well to the experimental values 3.25 Å and 5.20 Å, respectively.[36] In order to describe the electronic structure reasonably, we decide to modify α for all of our calculated oxides. The optimal values of α for each oxide are given in Table 1. The screening parameter is fixed at a value of 0.2 Å. The Monkhorst–Pack k-point meshes of $7 \times 7 \times 7$ for the B1 and B3 binary structures and $7 \times 7 \times 4$ for the B4 structure were employed.[37] The plane-wave cutoff energy of 450 eV is chosen to obtain converged results. All structures are fully relaxed until the force acting on each atom is less than 0.03 eV Å^{-1}.

The bulk binary structures were each optimized to their equilibrium volume through minimization of the total energy and stress. The bulk moduli (B) and the pressure derivative of the bulk moduli (B') were obtained by fitting the energy–volume data to the Murnaghan equation of state. In most cases, the main motivation of the study is not only the band structure *per se*, but also the band-gap variations with strain and/or alloy composition, *i.e.*, the band gap deformation potentials. The band gap volume-deformation potentials (α_V) and the pressure deformation potentials (α_P) were obtained from the relations

$$\alpha_V = \frac{\partial E_g}{\partial \ln V} \tag{1}$$

and

$$\alpha_P = -\left(\frac{1}{B}\right)\alpha_V, \tag{2}$$

respectively. As the information about the band alignment, *i.e.*, band lineup, is essential for the design of heterostructures, we summarize our results as determined by alignment to the oxygen 1s core electron energy level. We only considered the cubic B1 and B3 structures, because the differences between B3 and B4 electronic structures are small.[38,39] The alloy formation energies are calculated only in the B1 and B3 structures as well. The ternary random alloys $M_xZn_{1-x}O$ were modeled within 32-atom (16-mixed cation) supercells using the special quasi-random structure (SQS) approach to determine the cation-site occupancies.[40,41] In these SQSs, the averaged atomic correlation functions of the first and second neighbored pairs and triangles are all the same as the perfect random solid solution. The k-point meshes for the SQSs were tested to ensure good precision when comparing the total energies.

III. Results and discussion

A. Structural properties

The calculated structural parameters and energy differences of the B1, B3 and B4 structures are listed in Table 2. Some experimental data can be found in Table 1. It is found that, in the same structure, with increasing of the cation atomic number, the lattice constants become large because the cation atomic size increases. Among the calculated oxides, MgO has the closest lattice constants to ZnO. The lattice constant a of

Table 1 Experimental (ref. 24) and calculated equilibrium structural properties and electronic band gaps[a]

	Stable Phase	Expt.			Calc.			Band-gap type	α
		a (Å)	c/a	E_g (eV)	a (Å)	c/a	E_g (eV)		
BeO	B4	2.698	1.623	10.59	2.675	1.622	10.57	Direct	0.350
MgO	B1	4.216		7.90	4.160		7.91	Direct	0.385
CaO	B1	4.811		7.80	4.804		7.80	Indirect	0.595
SrO	B1	5.159		6.40	5.115		6.42	Indirect	0.510
BaO	B1	5.536		4.40	5.530		4.40	Direct	0.460
ZnO	B4	3.250	1.601	3.44	3.242	1.608	3.43	Direct	0.375
CdO	B1	4.689		0.84	4.709		0.84	Indirect	0.235

[a] α is the optimal portion of the non-local Fock-exchange energy in HSE06 functional.

Table 2 The calculated equilibrium structural properties and electronic band gaps of each oxide in the B1, B3 and B4 structures[a]

Phase	Material	a (Å)	c/a	ΔE (meV)	B (GPa)	B'	$E_g^{\Gamma-\Gamma}$ (eV)	E_g (eV)	Band-gap type
B1	BeO	2.540		984	276	4.01	11.84	11.40	Indirect
	MgO	2.941		0	179	4.14	7.91	7.91	Direct
	CaO	3.397		0	124	4.06	8.48	7.80	Indirect
	SrO	3.617		0	100	4.40	7.32	6.42	Indirect
	BaO	3.911		0	80	4.76	6.63	4.40	Direct
	ZnO	3.015		224	197	4.40	4.88	3.70	Indirect
	CdO	3.330		0	143	4.71	2.16	0.84	Indirect
B3	BeO	2.666		17	232	3.12	10.54	9.45	Indirect
	MgO	3.204		298	136	4.26	6.36	6.36	Direct
	CaO	3.706		610	83	3.96	7.22	6.73	Indirect
	SrO	3.914		402	71	4.43	6.47	5.49	Indirect
	BaO	4.185		162	56	4.22	6.10	4.72	Indirect
	ZnO	3.225		27	149	4.33	3.30	3.30	Direct
	CdO	3.594		73	104	4.71	0.93	0.93	Direct
B4	BeO	2.675	1.622	0	234	3.58	10.57	10.57	Direct
	MgO	3.267	1.527	221	135	3.96	6.22	6.22	Direct
	CaO	4.007	1.189	248	97	4.08	6.52	6.52	Direct
	SrO	4.234	1.203	154	81	4.37	5.63	5.63	Direct
	BaO	4.331	1.467	98	57	4.44	4.90	4.77	Indirect
	ZnO	3.242	1.608	0	149	4.36	3.43	3.43	Direct
	CdO	3.660	1.552	41	92	4.71	1.05	1.05	Direct

[a] The relative total energy (ΔE, meV) is given with respect to the most stable phase for each oxide.

MgO is just a little smaller than that of ZnO in the ionic B1 rock salt structure, while in the covalent B3 and B4 structures, it becomes a little larger than that of ZnO. As for other oxides, they have large lattice constants compared to ZnO except BeO and CdO. In the B4 wurtzite structure, the c/a ratio for all of the oxides is smaller than the ideal value $\sqrt{8/3} = 1.633$. The larger the atomic number is, the smaller the c/a ratio is. For each oxide in the B3 and B4 structures, the lattice constants are nearly the same, and the bulk moduli are almost identical. The B1 structure has relatively larger bulk moduli relative to the B3 and B4 structures because of its smaller volume. The stable phase for BeO and ZnO is the B4 structure. The energy differences between the B3 and B4 structures are 17 meV for BeO and 27 meV for ZnO, which are much smaller than those between the B1 and B4 structures, 984 meV and 224 meV, respectively. Due to the relatively larger energy difference between the B1 and B3 (B4) structures, other oxides steadily exist in the B1 structure. Our calculated structural properties

and phase stability for all the oxides agree well with the experimental results and previous theoretical studies.[42]

B. Band gaps

By optimizing the portion of the non-local Fock-exchange energy in HSE06 functional, the calculated band gaps are in good agreement with the experimental values. The experimental and calculated band gaps can be found in Tables 1 and 2, respectively. Fig. 2 shows some typical band structures in the B1, B3 and B4 structures. For group IIA and group IIB metal oxides in the same row, it can be found that the band gap of the former is larger. This is because the extra d electrons are introduced (such as Zn to Ca), or the d electrons are relatively higher in energy (such as Cd to Sr), which induces a strong p–d coupling with the oxygen 2p states,[43,44] *i.e.*, pushes the VBM up and decreases the band gap. For most oxides in the B1 structure, they have an indirect band gap except MgO and BaO.
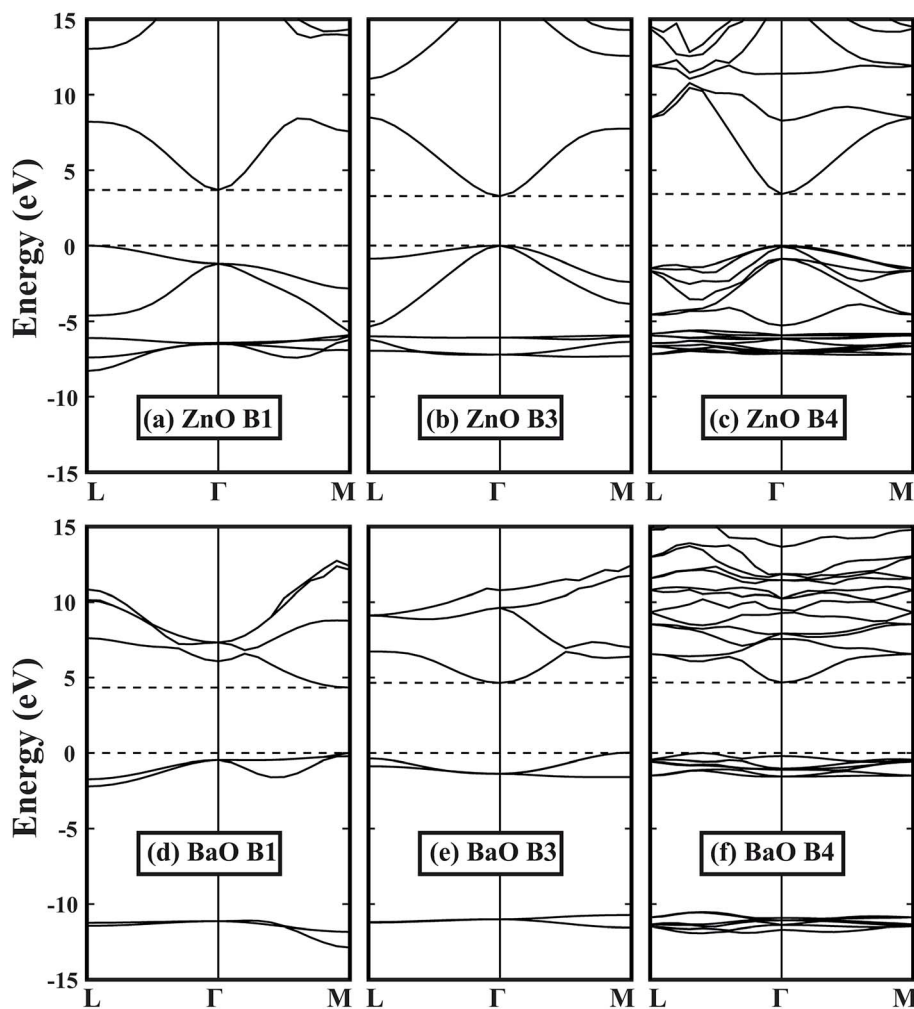
Fig. 2 Band structures of (a)–(c) ZnO and (d)–(f) BaO in the B1, B3 and B4 structures. Dashed lines indicate the VBM and CBM. All energies are relative to the VBM, *i.e.*, the energy value of VBM is set to zero.

However, it is totally different in the B4 structure: only the band gap of BaO is indirect, while others are all direct. This is due to the lack of repulse coupling between the occupied cation d states and oxygen 2p states at the Γ point in the B1 structure (O_h symmetry at the Γ point). Moreover, because the B1 structure has the smallest volume, it exhibits the largest band gap. As for the B3 and B4 structures, BeO, ZnO and CdO in the B4 structure have a slightly larger band gap relative to the B3 structure. This is due to the reduced symmetry in the B4 structure, which makes the level repulsion between the valence and conduction states stronger. However, for MgO, CaO, SrO and BaO, their band gaps in the B4 structure are relatively smaller than those in the B3 structure, which can be attributed to their much smaller c/a ratios, *i.e.*, the larger negative crystal field splitting at the VBM.

C. Band-gap deformation

Table 3 presents the calculated band-gap volume deformation potentials (α_V) and pressure deformation potentials (α_P). All the α_V are negative, while all the α_P are positive. As for different oxides in the same structure, when the cation gets bigger as the

atomic number of the cation increases, the cation–anion bond length becomes longer, which makes α_V become less negative. For each oxide in different structures, we can see that the B1 structure has an obvious larger absolute value of $\alpha_V^{\Gamma-\Gamma}$ because of its small volume. In the B3 and B4 structures, the values of $\alpha_V^{\Gamma-\Gamma}$ are very close except for BaO. For other gaps, such as $\Gamma-L$ and $\Gamma-X$, the values of $\alpha_V^{\Gamma-L}$ and $\alpha_V^{\Gamma-X}$ are also negative and the trend is similar to $\alpha_V^{\Gamma-\Gamma}$ with some minor value differences. The calculated results of the deformation potentials are consistent with the experimental results, although the values are a little bit underestimated.[45] It is worth pointing out that the band-gap volume deformation potentials for CdO are all negative in our calculations, which are quite different from those calculated by LDA and LAPW method,[46,47] indicating that HSE06 calculations give a better description of the deformation potentials.

The hydrostatic absolute deformation potentials of VBM and CBM are listed in Table 4. For each oxide, only the deformation potentials of the B1 and B3 structures are shown. Most of the α_{VBM} are positive. This is because that, at the valence band, there is a strong coupling between the anion occupied p states and the cation empty p states, *i.e.*, a strong positive volume-deformation term. As for BeO, the absolute deformation

Table 3 Calculated band-gap volume-deformation potentials (α_V, eV) and pressure coefficients (α_P, meV kbar^{-1})

	Phase	$\alpha_V^{\Gamma-\Gamma}$	$\alpha_P^{\Gamma-\Gamma}$	$\alpha_V^{\Gamma-L}$	$\alpha_P^{\Gamma-L}$	$\alpha_V^{\Gamma-X}$	$\alpha_P^{\Gamma-X}$
BeO	B1	−17.77	6.44	−8.42	3.05	−11.81	4.28
	B3	−11.85	5.10	−11.61	5.00	−2.31	0.99
	B4	−11.87	5.07	−11.72	5.00	−5.29	2.26
MgO	B1	−11.63	6.48	−7.36	4.10	−1.79	1.00
	B3	−6.76	4.98	−8.28	6.11	−3.16	2.33
	B4	−6.51	4.83	−7.44	5.52	−5.00	3.71
CaO	B1	−9.53	7.70	−6.38	5.16	−0.72	0.58
	B3	−6.12	7.36	−6.37	7.66	−4.69	5.64
	B4	−4.30	4.44	−4.71	4.86	−3.74	3.58
SrO	B1	−9.32	9.34	−5.44	5.45	−0.69	0.97
	B3	−6.04	8.54	−6.09	8.61	−5.39	7.62
	B4	−4.02	4.99	−4.38	5.43	−3.20	3.97
BaO	B1	−9.03	11.25	−4.43	5.52	−0.17	0.21
	B3	−5.88	10.46	−5.70	10.14	−5.73	10.20
	B4	−1.73	3.06	−2.40	4.25	−1.09	1.93
ZnO	B1	−10.03	5.10	−6.28	3.19	−9.61	4.89
	B3	−2.46	1.65	−4.91	3.30	−0.81	0.54
	B4	−2.55	1.71	−3.59	2.41	−2.43	1.63
CdO	B1	−6.65	4.63	−5.04	3.51	−9.00	6.27
	B3	−0.16	0.15	−3.31	3.17	−0.91	0.87
	B4	−0.28	0.31	−1.74	1.90	−2.23	2.43

Table 4 Calculated hydrostatic absolute deformation potentials (eV) of the Γ centered VBM and CBM states of each oxide in the B1 and B3 structures

	Phase	α_{VBM}	α_{CBM}
BeO	B1	−0.68	−18.47
	B3	−0.49	−12.81
MgO	B1	0.47	−11.17
	B3	1.38	−5.36
CaO	B1	1.04	−8.46
	B3	2.47	−3.64
SrO	B1	1.09	−8.22
	B3	2.65	−3.40
BaO	B1	1.20	−7.85
	B3	2.66	−3.24
ZnO	B1	1.12	−8.90
	B3	−2.82	−5.28
CdO	B1	1.61	−5.04
	B3	−2.40	−2.56

D. Band edge alignment

In order to analyze the calculated natural band alignments for the B1 and B3 structures, we set the VBM of BeO to zero, see Fig. 3(a) and (b). In both the B1 and B3 structures, the VBM has an obvious decrease from BeO to MgO to CaO, then it goes up from SrO to BaO to ZnO to CdO. As there are semi-core d electrons in Sr, Ba, Zn and Ca, the interaction between the anion p and the occupied cation d states results in a level repulsion, moving the VBM upwards. Although Cd has deeper d states and weaker p–d coupling than Zn, the large lattice constant of CdO contributes to its higher VBM compared to ZnO. These reproduce the trends previously established for II–VI semiconductors.[48] The VBM contains some indirect components in BaO, ZnO and CdO in the B1 structure, which can be attributed to that this particular p–d coupling is restricted at Γ point in O_h symmetry. For the B3 structure, the trend is similar to that in the B1 structure: the indirect components appear in CaO, SrO and BaO instead of ZnO and CdO due to the different symmetry in the B3 structure.

The heterostructural offsets of the stable phases of each oxide are illustrated in Fig. 3(c). The band offset from B3 BeO to B1 MgO is −3.92 eV, which is more negative than the band offset from B3 BeO to B3 MgO (−2.08 eV), indicating that the VBM of B1 MgO is lower than that of B3 MgO. The same phenomenon can be found in other oxides, such as CaO, SrO and BaO. This is because that the relatively short bond length in the B1 structure enhances the interaction between the cation and the anion,
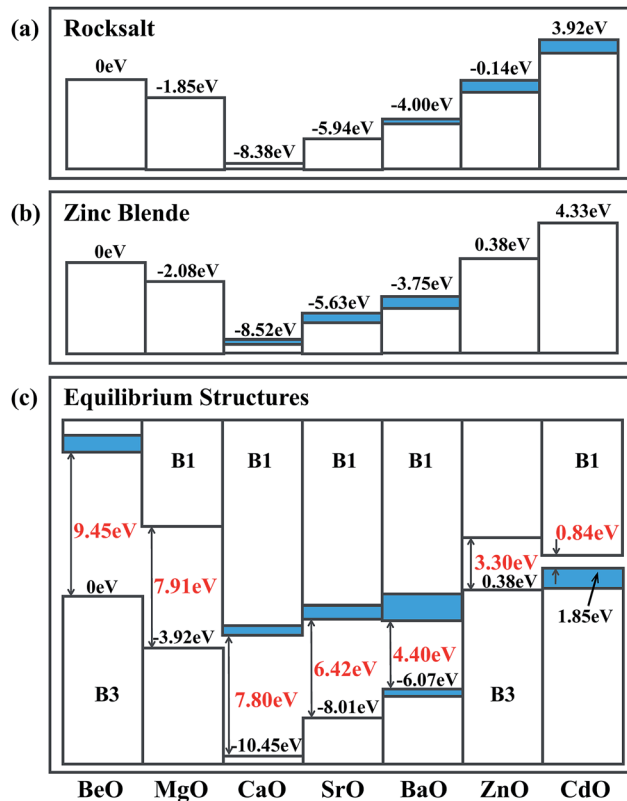
Fig. 3 The calculated natural band alignments in the (a) B1 and (b) B3 crystal structures. The heterostructural offsets are shown in (c). Indirect contributions to the valence band are colored blue.

potentials of the VBM are negative. The kinetic energy effects, which contribute a negative volume-deformation term for the VBM, should play a key role in BeO due to its small volume. However, for ZnO and CdO, the deformation potentials of the VBM in the B1 structure are positive, while they become negative in the B3 structure. This is due to the fact that when the cation has shallow occupied d states, the repulse coupling between the anion p states and the cation d states will occur at the Γ point in the B3 structure, which produces negative effect in the deformation potentials of the VBM. Plus, the kinetic energy effects also have some negative contributions to the deformation potentials of the VBM here. For the conduction band, all the α_{CBM} are negative due to the strong negative contributions from the antibonding repulsion between anion s and cation s, and from the kinetic energy effects.

which results in the expansion of the band gap and the reduction of the VBM compared with that in the B3 structure.

E. Ternary alloy formation

The ternary random alloys $M_xZn_{1-x}O$ formed by ZnO and other group II metal oxides were investigated in both the B1 and B3 structures. In our calculations, we constructed only one M_x-$Zn_{1-x}O$ SQS with $x = 0.5$ for each oxide. The calculated structural and electronic properties are summarized in Table 5. Obviously, the lattice mismatch is highly related to the atomic size difference of the cations. The size of Mg atom is close to that of Zn atom, so the lattice mismatch between them is small. When the atomic size significantly increases from Ca to Sr to Ba, the corresponding lattice mismatch is getting larger and larger. The lattice mismatch in the B1 structure is slightly smaller than that in the B3 structure because the B3 structure has a relatively large volume. The ternary alloy formation energy (ΔH) at 50% composition is defined as follows,

$$\Delta H = E(Zn_{0.5}M_{0.5}O) - \frac{1}{2}[E(ZnO) + E(MO)]. \quad (3)$$

The calculated results can be found in Table 5. The formation energy of (Zn, Mg)O shows smaller absolute values in both the B1 and B3 structures due to the small lattice mismatch and attractive chemical interactions.[49] For (Zn, Ca)O in the B1 and B3 structures, the formation energies are 17.45 meV and −185.04 meV, respectively. In the B1 structure, the formation energy (Be, Zn)O is also negative. B3 (Mg, Zn)O exhibits a slightly negative formation energy, too. Similar negative formation energies have been reported for Mg and Zn lithium nitride alloy.[50] For other alloys, all the formation energy are positive, and it is obvious that the formation energy is much larger in the B1 structure than that in the B3 structure except for (Be, Zn)O. This is due to the relatively lower symmetry for the B3 structure, which facilitates the structural relaxation and Coulomb binding, *i.e.*, reduces the strain in the alloy.

We also calculated the band-gap bowing, b, which is used to describe the deviation away from the linear interpolation of the component band gaps. It was calculated according to the following equation,

Table 5 Alloy lattice mismatch ($\Delta a/a$, %), formation energy (ΔH, meV) and band-gap bowing parameters (b, eV)

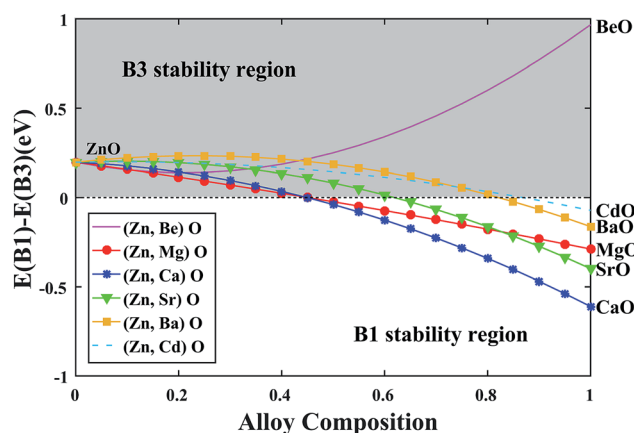|	Phase	$\Delta a/a$ (%)	ΔH (meV)	b (eV)
(Be, Zn)O	B1	16.43	−52.82	15.94
	B3	18.98	279.68	6.58
(Mg, Zn)O	B1	2.42	6.87	3.62
	B3	0.62	−18.00	1.97
(Ca, Zn)O	B1	11.73	−17.45	2.32
	B3	13.62	−185.04	0.80
(Sr, Zn)O	B1	18.35	247.46	3.36
	B3	19.19	64.36	0.29
(Ba, Zn)O	B1	26.62	239.60	0.17
	B3	25.84	71.42	0.06
(Cd, Zn)O	B1	9.68	164.55	2.80
	B3	10.74	83.74	1.10

Fig. 4 Energetic stability of the B1 and B3 structures as a function of alloy composition.

$$E_g^{alloy}(x) = (1 - x)(E_g^{ZnO}) + x(E_g^{MO}) - bx(1 - x). \quad (4)$$

Table 5 shows the calculated results. For all the alloys, the band-gap bowing in the B1 structure is significantly larger than that in the B3 structure because of the higher symmetry and shorter bond length in the B1 structure. The band-gap bowing of (Zn, Ba)O is the smallest. It is only 0.17 eV in the B1 structure and 0.06 eV in the B3 structure, indicating that the band gap of (Zn, Ba)O alloy has almost linear interpolation of the component band gap. Similarly, the phase stability of each alloy can be estimated by calculating the total energy of each component and $Zn_{0.5}M_{0.5}O$ alloy, *i.e.*,

$$E_{B1-B3}^{alloy}(x) = (1 - x)(E_{B1-B3}^{ZnO}) + x(E_{B1-B3}^{MO}) - x(\Omega_{B1-B3})(1 - x). \quad (5)$$

After obtaining the compositionally independent interaction energy (Ω) *via* setting the $x = 0.5$ in eqn (5), we can draw a curve to predict the phase stability of the alloy over a wider compositional range. As shown in Fig. 4, we can see that the stable phase is always B3 over the entire compositional range for (Zn, Be)O alloy. This is because both ZnO and BeO steadily exist in the B3 structure. For other alloys, the stable phase is B3 at the beginning, while with the decrease of the ZnO composition, the stable phase turns to the B1 structure. The critical point of the transition gradually increases from (Ca, Zn)O to (Mg, Zn)O to (Sr, Zn)O to (Ba, Zn)O to (Cd, Zn)O, indicating that (Ca, Zn)O can exist in the B3 structure with the lowest ZnO composition.

IV. Conclusions

In this work, we have obtained the optimal portion of the non-local Fock-exchange energy within HSE06 by comparing the calculated band gaps with the experimental values for all group II metal oxides MO (M = Be, Mg, Ca, Sr, Ba, Zn, Cd) in their stable phases. Then, the geometric and electronic structure of all the oxides have been calculated in the B1, B3 and B4 structures. The ground state properties like the lattice constants, band gaps and formation energies have a good agreement with the experimental results. The band-gap volume-deformation generally decreases with the increase of the cation atomic

number. By analyzing the band-edge alignment, we found that in both the B1 and B3 structures, the VBM has an obvious decrease from BeO to MgO to CaO, then it goes up from SrO to BaO to ZnO to CdO. The lattice mismatch, band-gap bowing parameter and formation energy of ternary alloy $M_xZn_{1-x}O$ were also studied through the application of the special quasi-random structure method. The phase transition from the B1 structure to the B3 structure is predicted with decreasing of the ZnO composition. The critical point of the transition gradually increases from (Ca, Zn)O to (Mg, Zn)O to (Sr, Zn)O to (Ba, Zn)O to (Cd, Zn)O, indicating that (Ca, Zn)O can exist in the B3 structure with the lowest ZnO composition. These results provide a good guideline for the accessible phase space in these alloy systems.

Conflicts of interest

There are no conflicts to declare.

Acknowledgements

References

1 C. Ma, W. Jin, X. Duan, X. Ma, H. Han, Z. Zhang, J. Yu and Y. Wu, *J. Alloys Compd.*, 2019, **772**, 482–488.

2 X. Duan, C. Ma, W. Jin, X. Ma, L. Guo, S.-H. Wei, J. Yu and Y. Wu, *Phys. Chem. Chem. Phys.*, 2018, **20**, 18455–18462.

3 Q. Wang, A. R. Oganov, Q. Zhu and X.-F. Zhou, *Phys. Rev. Lett.*, 2014, **113**, 266101.

4 G. Mattioli, A. A. Bonapasta, D. Bovi and P. Giannozzi, *J. Phys. Chem. C*, 2014, **118**, 29928–29942.

5 T. de Boer, M. F. Bekheet, A. Gurlo, R. Riedel and A. Moewes, *Phys. Rev. B: Condens. Matter Mater. Phys.*, 2016, **93**, 155205.

6 W. J. Yin, J. Ma, S. H. Wei, M. M. Al-Jassim and Y. F. Yan, *Phys. Rev. B: Condens. Matter Mater. Phys.*, 2012, **86**, 045211.

7 G. S. Chang, J. Forrest, E. Z. Kurmaev, A. N. Morozovska, M. D. Glinchuk, J. A. McLeod, A. Moewes, T. P. Surkova and N. H. Hong, *Phys. Rev. B: Condens. Matter Mater. Phys.*, 2012, **85**, 165319.

8 H. Fujiwara and M. Kondo, *Phys. Rev. B: Condens. Matter Mater. Phys.*, 2005, **71**, 075109.

9 C. X. Kronawitter, M. Kapilashrami, J. R. Bakke, S. F. Bent, C.-H. Chuang, W.-F. Pong, J. Guo, L. Vayssieres and S. S. Mao, *Phys. Rev. B: Condens. Matter Mater. Phys.*, 2012, **85**, 125109.

10 J. T-Thienprasert, S. Rujirawat, W. Klysubun, J. N. Duenow, T. J. Coutts, S. B. Zhang, D. C. Look and S. Limpijumnong, *Phys. Rev. Lett.*, 2013, **110**, 055502.

11 R. Gillen and J. Robertson, *Phys. Rev. B: Condens. Matter Mater. Phys.*, 2011, **84**, 035125.

12 A. Soon, M. Todorova, B. Delley and C. Stampfl, *Phys. Rev. B: Condens. Matter Mater. Phys.*, 2007, **75**, 125420.

13 T. Dietl and H. Ohno, *Rev. Mod. Phys.*, 2014, **86**, 187–251.

14 A. De and C. E. Pryor, *Phys. Rev. B: Condens. Matter Mater. Phys.*, 2010, **81**, 155210.

15 J. L. Birman, *Phys. Rev.*, 1959, **115**, 1493–1505.

16 F. Luo, Y. Cheng, L.-C. Cai and X.-R. Chen, *J. Appl. Phys.*, 2013, **113**, 033517.

17 C.-J. Park, S.-G. Lee, Y.-J. Ko and K. J. Chang, *Phys. Rev. B: Condens. Matter Mater. Phys.*, 1999, **59**, 13501–13504.

18 A. Ashrafi and C. Jagadish, *J. Appl. Phys.*, 2007, **102**, 071101.

19 M. A. Gluba, N. H. Nickel and N. Karpensky, *Phys. Rev. B: Condens. Matter Mater. Phys.*, 2013, **88**, 245201.

20 H. Hung-Chun Lai, V. L. Kuznetsov, R. G. Egdell and P. P. Edwards, *Appl. Phys. Lett.*, 2012, **100**, 072106.

21 D. M. Detert, S. H. M. Lim, K. Tom, A. V. Luce, A. Anders, O. D. Dubon, K. M. Yu and W. Walukiewicz, *Appl. Phys. Lett.*, 2013, **102**, 232103.

22 A. J. Cinthia, G. S. Priyanga, R. Rajeswarapalanichamy and K. Iyakutti, *J. Phys. Chem. Solids*, 2015, **79**, 23–42.

23 A. JemmyCinthia, G. Sudhapriyang, R. Rajeswarapalanichamy and M. Santhosh, *Procedia Mater. Sci.*, 2014, **5**, 1034–1042.

24 O. Madelung, *Semiconductors: Data Handbook*, Springer, Berlin, Heidelberg, 2004.

25 S. Baroni, S. de Gironcoli, A. Dal Corso and P. Giannozzi, *Rev. Mod. Phys.*, 2001, **73**, 515–562.

26 G. Kresse and J. Hafner, *Phys. Rev. B: Condens. Matter Mater. Phys.*, 1993, **48**, 13115–13118.

27 P. Hohenberg and W. Kohn, *Phys. Rev.*, 1964, **136**, B864–B871.

28 G. Kresse and J. Furthmüller, *Phys. Rev. B: Condens. Matter Mater. Phys.*, 1996, **54**, 11169–11186.

29 G. Kresse and D. Joubert, *Phys. Rev. B: Condens. Matter Mater. Phys.*, 1999, **59**, 1758–1775.

30 A. V. Krukau, O. A. Vydrov, A. F. Izmaylov and G. E. Scuseria, *J. Chem. Phys.*, 2006, **125**, 224106.

31 J. P. Perdew, K. Burke and M. Ernzerhof, *Phys. Rev. Lett.*, 1996, **77**, 3865–3868.

32 J. P. Perdew, K. Burke and M. Ernzerhof, *Phys. Rev. Lett.*, 1997, **78**, 1396.

33 J. Heyd, G. E. Scuseria and M. Ernzerhof, *J. Chem. Phys.*, 2003, **118**, 8207–8215.

34 J. Heyd, G. E. Scuseria and M. Ernzerhof, *J. Chem. Phys.*, 2006, **124**, 219906.

35 K. Nagamoto, K. Kato, S. Naganawa, T. Kondo, Y. Sato, H. Makino, N. Yamamoto and T. Yamamoto, *Thin Solid Films*, 2011, **520**, 1411–1415.

36 U. Özgür, Y. I. Alivov, C. Liu, A. Teke, M. A. Reshchikov, S. Doğan, V. Avrutin, S.-J. Cho and H. Morkoç, *J. Appl. Phys.*, 2005, **98**, 041301.

37 H. J. Monkhorst and J. D. Pack, *Phys. Rev. B: Condens. Matter Mater. Phys.*, 1976, **13**, 5188–5192.

38 S.-H. Wei and A. Zunger, *Phys. Rev. B: Condens. Matter Mater. Phys.*, 1999, **60**, 5404–5411.

39 S.-H. Wei and A. Zunger, *Appl. Phys. Lett.*, 1996, **69**, 2719–2721.

40 A. Zunger, S.-H. Wei, L. G. Ferreira and J. E. Bernard, *Phys. Rev. Lett.*, 1990, **65**, 353–356.

41 S.-H. Wei, L. G. Ferreira, J. E. Bernard and A. Zunger, *Phys. Rev. B: Condens. Matter Mater. Phys.*, 1990, **42**, 9622–9649.

42 A. Schleife, F. Fuchs, J. Furthmüller and F. Bechstedt, *Phys. Rev. B: Condens. Matter Mater. Phys.*, 2006, **73**, 245212.

43 S.-H. Wei and A. Zunger, *Phys. Rev. B: Condens. Matter Mater. Phys.*, 1988, **37**, 8958–8981.

44 Y. Wu, G. Chen, S.-H. Wei, M. Al-Jassim and Y. Yan, *Phys. Rev. B: Condens. Matter Mater. Phys.*, 2012, **86**, 155205.

45 J. Huso, J. L. Morrison, H. Hoeck, X.-B. Chen, L. Bergman, S. J. Jokela, M. D. McCluskey and T. Zheleva, *Appl. Phys. Lett.*, 2006, **89**, 171909.

46 Y. Z. Zhu, G. D. Chen, H. Ye, A. Walsh, C. Y. Moon and S.-H. Wei, *Phys. Rev. B: Condens. Matter Mater. Phys.*, 2008, **77**, 245209.

47 Y.-H. Li, X. Gong and S.-H. Wei, *Appl. Phys. Lett.*, 2006, **88**, 042104.

48 S.-H. Wei and A. Zunger, *Appl. Phys. Lett.*, 1998, **72**, 2011–2013.

49 M. Sanati, G. L. W. Hart and A. Zunger, *Phys. Rev. B: Condens. Matter Mater. Phys.*, 2003, **68**, 155210.

50 A. Walsh and S.-H. Wei, *Phys. Rev. B: Condens. Matter Mater. Phys.*, 2007, **76**, 195208.